ELSEVIER

Journal of Power Sources 93 (2001) 230–233

JOURNAL OF POWER SOURCES

www.elsevier.com/locate/jpowsour

Effect of cerium on the anodic corrosion of Pb–Ca–Sn alloy in sulfuric acid solution

Hou-Tian Liu*, Jiong Yang, Hai-He Liang, Ji-Hua Zhuang, Wei-Fang Zhou

Chemistry Department, Fudan University, Shanghai 200433, PR China

Received 8 May 2000; received in revised form 7 August 2000; accepted 1 September 2000

Abstract

The anodic corrosion of Pb–0.10 wt.% Ca–0.88 wt.% Sn alloy and Pb–0.10 wt.% Ca–0.88 wt.% Sn–0.048 wt.% Ce alloy in 4.5 M H_2SO_4 at 20°C was studied using cyclic voltammetry, linear sweep voltammetry, ac voltammetry, chronoamperometry, and scanning electron microscopy. The experimental results show that the cerium added to Pb–Ca–Sn alloy inhibits the growth of the anodic corrosion layer and reduces the resistivity of the anodic Pb(II) film.

Keywords: Pb–Ca–Sn–Ce alloy; Lead–acid battery; Cerium; Anodic Pb(II) film

1. Introduction

The lead alloys generally used as positive grids in lead–acid batteries are Pb–Sb and Pb–Ca alloys [1–3]. It was reported that Pb–Sb alloy is corroded and the complex antimony ions are formed as oxidized species during normal battery operation [4]. This complex antimony ions slowly migrate through the positive active material and the electrolyte and, then, antimony deposits on the negative electrode, lowering the overpotential of hydrogen evolution, and the adverse effects could occur: (i) increased self-discharge; (ii) excessive water loss or increased maintenance; (iii) decreased charge efficiency. Calcium increases the overpotential of hydrogen evolution on lead alloy and results in improving the performance of maintenance-free for the batteries. But the lead–calcium alloy has poor strength and casting performance. Especially, a high-impedence 'passivation' layer formed on Pb–Ca alloy during anodization can give rise to the detrimental influences on the deep charge/discharge cycle performance of the batteries [5–6]. Now, one of the most effective methods is to add tin into the lead alloy to improve the conductivity of the anodic film. However, the deep charge/discharge cycle performance of Pb–Ca–Sn is still not satisfactory. Moreover, tin dissolves in the electrolyte from the alloy and forms Sn^{2+}. The reaction of Sn^{2+}/Sn^{4+} redox couple with the active materials of the positive and negative electrodes may increase the self-discharge of the batteries [7–8].

Owing to the mentioned detrimental influences of Pb–Ca alloy, some metal elements, such as strontium or lithium, whose electrode potential is close or more negative than that of calcium, have been added into lead or lead alloys to improve the crystal grain structure of the alloys and not obviously decrease the hydrogen overpotential [9–12]. Cerium also has the value of the electrode potential close to that of calcium. Although the overpotential for hydrogen evolution on cerium is slightly lower than that on calcium [13], cerium has higher hardness and better mechanical performance than lead, calcium, strontium and lithium. So far, cerium is often used as fine crystal grain improver of alloys to enhance the corrosion and abrasion resistance in the metallurgy industry. It has not been reported that there is any new positive grid made of Pb–Ca–Sn alloy containing cerium for maintenance-free lead–acid batteries. In the present work, the anodic corrosion of Pb–Ca–Sn alloy containing cerium in sulfuric acid solution was studied to clarify the possibility of Pb–Ca–Sn alloy containing cerium as a candidate for the positive grid material.

2. Experimental

A lead–0.10 wt.% calcium–0.88 wt.% tin alloy (Pb–Ca–Sn) rod and a lead–0.10 wt.% calcium–0.88 wt.% tin–0.048 wt.% cerium alloy (Pb–Ca–Sn–Ce) rod were used as working electrodes. The alloys were manufactured by

* Corresponding author. Fax: +86-21-6564-1740.
E-mail address: htliuk@online.sh.cn (H.-T. Liu).

0378-7753/01/$ – see front matter
PII: S0378-7753(00)00583-8

Shanghai High Power Storage Battery Factory with lead (99.99%), calcium (99.5%), tin (99.9%) and cerium (99.9%). Both Pb–Ca–Sn and Pb–Ca–Sn–Ce rods were shelved at room temperature for 2 weeks before carrying out experiment. The rods were sealed with epoxy resin in the lower part of an L-shaped glass tube, so that a cross sectional area of 0.28 cm^2 was exposed in the electrolyte. A flat working-electrode surface was obtained by mechanical polishing with emery paper of successively decreasing grain size down to about 10 μm. The working electrodes were, then, washed with double-distilled water before immersed in the electrolyte. Before every experiment, a cathodic polarization at a potential of −1.2 V for 20 min was performed in order to remove any oxidation products formed by aerial oxidation during preliminary treatment. The electrolyte was 4.5 M H_2SO_4 solution prepared from A.R. H_2SO_4 and double-distilled water. A platinum plate served as a counter electrode. An Hg/Hg_2SO_4 electrode containing the same solution in the electrochemical cell was used as the reference electrode. All potentials reported here are referred to this electrode.

Cyclic voltammetry and ac voltammetry were carried out using CH Instrument Model 660 Electrochemical Working Station. Linear sweep voltammetry was performed using an EG&G PARC 273 Potentiost-Galvanostat controlled by EG&G PARC Model 270 software.

The electron micrographs of the corrosion layers were obtained using HITACHI S-50 scanning electron microscope (SEM). All electrochemical measurements were performed at 20 ± 1°C.

3. Results and discussion

3.1. Cyclic voltammetry

Fig. 1 illustrates the cyclic voltammograms of Pb–Ca–Sn and Pb–Ca–Sn–Ce electrodes for the 100th cycle performed between 0.6 and 1.4 V at a sweep rate of 5 mV s^{-1} in 4.5 M H_2SO_4 solution. In the positive sweep, two anodic peaks a and b are observed, they correspond to the formation of PbO_2 and the oxygen evolution, respectively. In the negative sweep, the cathodic peak c appears, which corresponds to the reduction of PbO_2. From Fig. 1, it can be found that the potential of peak a of Pb–Ca–Sn–Ce (1.09 V) is more positive than that of Pb–Ca–Sn (1.07 V) and the peaks a, b and c of Pb–Ca–Sn–Ce are all shorter than those of Pb–Ca–Sn. It suggests that the addition of cerium inhibits the growth of the anodic PbO_2film.

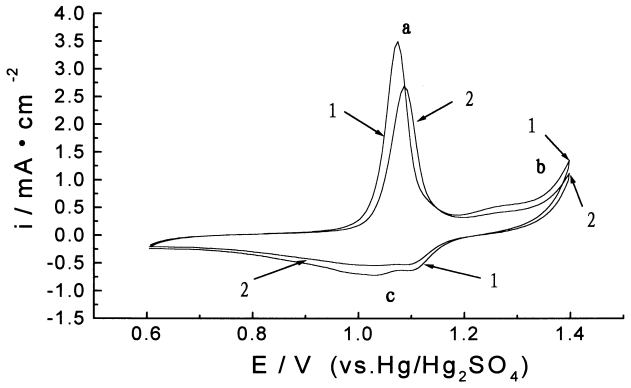

Fig. 1. Cyclic voltammograms at 100th cycle for Pb–Ca–Sn (1) and Pb–Ca–Sn–Ce (2) electrodes in 4.5 M H_2SO_4, ($v = 5$ mV s^{-1}), $T = 20$°C.

Table 1 lists the anodic oxidation charges (Q_{ox}) and cathodic reduction charges (Q_{red}) in the cyclic voltammograms for Pb–Ca–Sn and Pb–Ca–Sn–Ce electrodes. From the nearly constant value of ($Q_{ox} - Q_{red}$), it is considered that the difference between Q_{ox} and Q_{red} may be mainly due to the anodic evolution of oxygen. According to the value of ($Q_{ox} - Q_{red}$), it can be concluded that the addition of cerium may increase the overpotential of oxygen evolution. It is observed that there is a good linear relationship between Q_{red} and the cyclic number (N). The increase rate of reduction charges of Pb–Ca–Sn–Ce alloy is 3.30×10^{-4} C cm^{-2} $cycle^{-1}$, obviously less than that of Pb–Ca–Sn, 4.42×10^{-4} C cm^{-2} $cycle^{-1}$. Hence, the addition of cerium may enhance the corrosion resistance of the lead alloy.

3.2. Liner sweep voltammetry

The electrodes were anodized at 0.9 V with 15, 30, 60, 90 and 120 min, and then swept to −1.2 V at a rate of 2 mV s^{-1}

Table 1
Comparison of the anodic oxidation charges (Q_{ox}) and cathodic reduction (Q_{red}) charges in cyclic voltammograms for Pb–Ca–Sn (1) and Pb–Ca–Sn–Ce (2) electrodes

Cycles (N)	Pb–Ca–Sn			Pb–Ca–Sn–Ce		
	Q_{ox} (C cm^{-2})	Q_{red} (C cm^{-2})	$Q_{ox} - Q_{red}$ (C cm^{-2})	Q_{ox} (C cm^{-2})	Q_{red} (C cm^{-2})	$Q_{ox} - Q_{red}$ (C cm^{-2})
30	5.23×10^{-2}	2.10×10^{-2}	3.13×10^{-2}	4.07×10^{-2}	1.84×10^{-2}	2.23×10^{-2}
40	5.97×10^{-2}	2.58×10^{-2}	3.39×10^{-2}	4.55×10^{-2}	2.33×10^{-2}	2.21×10^{-2}
50	6.61×10^{-2}	3.06×10^{-2}	3.55×10^{-2}	5.04×10^{-2}	2.73×10^{-2}	2.31×10^{-2}
60	7.12×10^{-2}	3.51×10^{-2}	3.61×10^{-2}	5.50×10^{-2}	3.06×10^{-2}	2.44×10^{-2}
70	7.57×10^{-2}	3.93×10^{-2}	3.64×10^{-2}	5.91×10^{-2}	3.33×10^{-2}	2.58×10^{-2}
80	7.99×10^{-2}	4.39×10^{-2}	3.60×10^{-2}	6.38×10^{-2}	3.64×10^{-2}	2.74×10^{-2}
90	8.37×10^{-2}	4.81×10^{-2}	3.56×10^{-2}	6.80×10^{-2}	3.95×10^{-2}	2.85×10^{-2}
100	8.72×10^{-2}	5.18×10^{-2}	3.54×10^{-2}	7.22×10^{-2}	4.22×10^{-2}	3.00×10^{-2}

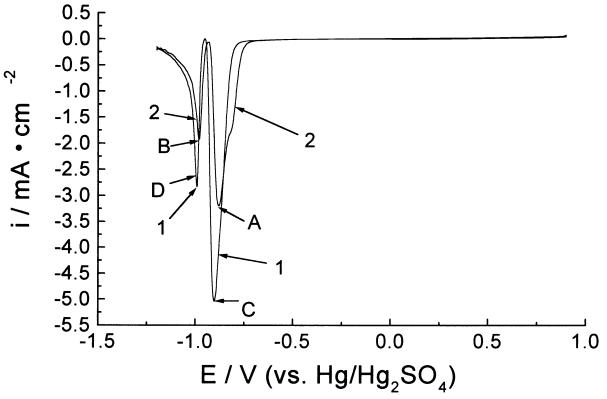

Fig. 2. Voltammograms of anodic films formed on Pb–Ca–Sn (1) and Pb–Ca–Sn–Ce (2) electrodes at 0.9 V for 1 h in 4.5 M H_2SO_4 ($v = 2$ mV s^{-1}), $T = 20°C$.

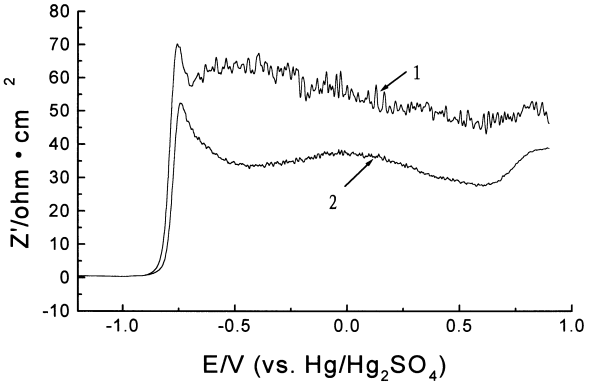

Fig. 3. Z' vs. E plot of the anodic Pb(II) films formed on Pb–Ca–Sn (1) and Pb–Ca–Sn–Ce (2) electrodes at 0.9 V in 4.5 M H_2SO_4 for 1 h, $T = 20°C$ ($v = 2$ mV s^{-1}, $f = 1000$ Hz).

in 4.5 M H_2SO_4 solution. The potential 0.9 V was chosen for the anodic film growth**,** because it is close to the potential of the positive grid after the deep discharge for the batteries. Fig. 2 shows the voltammograms of the anodic films of Pb–Ca–Sn and Pb–Ca–Sn–Ce formed at 0.9 V for 1 h. The potentials of the peak A (−0.88 V) and the peak B (−0.98 V) for Pb–Ca–Sn–Ce in curve (2) are less negative than those of the peak C (−0.90 V) and the peak D (−0.99 V) for Pb–Ca–Sn in curve (1), respectively. It can be considered that the peaks A and C correspond to the reduction of $PbO + PbO{\cdot}PbSO_4$ (Pb(II)) to Pb, the peaks B and D correspond to the reduction of $PbSO_4$ to Pb [14]. It shows that the addition of cerium is probably beneficial to decrease the reduction overpotential of Pb(II) and $PbSO_4$to Pb. The peak current of $PbSO_4$/Pb reaction does not vary significantly with the anodization time if the anodization time is longer than 15 min. But the peak current of Pb(II)/Pb reaction increases with the oxidation time.

Table 2 lists the reduction charges for the Pb(II)/Pb and the $PbSO_4$/Pb peaks in the linear sweep voltammograms for the anodic films on the Pb–Ca–Sn and Pb–Ca–Sn–Ce electrodes formed at 0.9 V. It can be inferred from Table 2 that after 15 min the thickness of the $PbSO_4$ film was almost invariable. It can be observed from Table 2 that the increase rates of the reduction charges for the Pb(II)/Pb peaks of the Pb–Ca–Sn and Pb–Ca–Sn–Ce electrodes are 3.35×10^{-5} and 2.66×10^{-5} C cm^{-2} s^{-1}, respectively. Hence, the addition of cerium into Pb–Ca–Sn alloy can obviously inhibit the growth of the anodic Pb(II) film. As Pb(II) is the major component of the anodic film, it may be concluded that cerium can improve the corrosion resistance of the lead alloys.

3.3. The real part of the impedance for the anodic Pb(II) films

Since the resistivity of the PbO crystal is quite high, about 10^{11} Ω cm [1], the high impedance of the anodic Pb(II) film greatly influences the deep charge/discharge performance of the battery. The variation of the impedance with negative linear potential sweep for the anodic film has been measured by the ac voltammetry. Fig. 3 shows the Z' (real part of the impedance) versus E plots of the anodic films formed on Pb–Ca–Sn and Pb–Ca–Sn–Ce electrodes at 0.9 V in 4.5 M H_2SO_4 solution for 1 h. It can be observed that Z' decreases obviously at the potentials of −0.77 and −0.74 V for Pb–Ca–Sn and Pb–Ca–Sn–Ce electrodes, respectively, and this corresponds to the impedance variation of the high resistive Pb(II) films to the electric conductive Pb. In comparison of the curve 1 with the curve 2 in Fig. 3, it can be found that Z' of Pb–Ca–Sn–Ce electrode is obviously less than that of Pb–Ca–Sn. It suggests that the additive cerium may reduce the resistivity of the anodic Pb(II) film.

3.4. Current–time curve at 0.9 V for positive grids

The positive grids of 1.6 cm × 6.0 cm made of Pb–Ca–Sn and Pb–Ca–Sn–Ce alloys were anodized for 30 days. Fig. 4

Table 2
Comparison for the reduction charges in the voltammograms for the anodic Pb(II) films of Pb–Ca–Sn and Pb–Ca–Sn–Ce electrodes

		Anodization time (min)				
		15	30	60	90	120
Pb–Ca–Sn	$Q_{Pb(II)/Pb}$ (C cm^{-2})	-8.43×10^{-2}	-1.12×10^{-1}	-1.84×10^{-1}	-2.34×10^{-1}	-2.95×10^{-1}
	$Q_{PbSO4/Pb}$ (C cm^{-2})	-7.65×10^{-2}	-8.09×10^{-2}	-8.84×10^{-2}	-8.05×10^{-2}	-8.71×10^{-2}
Pb–Ca–Sn–Ce	$Q_{Pb(II)/Pb}$ (C cm^{-2})	-6.43×10^{-2}	-9.63×10^{-2}	-1.49×10^{-1}	-1.95×10^{-1}	-2.32×10^{-1}
	$Q_{PbSO4/Pb}$ (C cm^{-2})	-6.55×10^{-2}	-7.50×10^{-2}	-7.86×10^{-2}	-8.18×10^{-2}	-8.48×10^{-2}

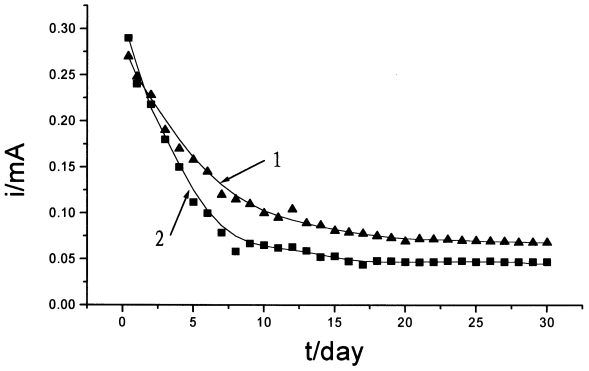

Fig. 4. Current–time plot for Pb–Ca–Sn (1) and Pb–Ca–Sn–Ce (2) grids at 0.9 V in 4.5 M H_2SO_4, $T = 20^{\circ}C$.

is the *i–t* curves for Pb–Ca–Sn and Pb–Ca–Sn–Ce grids at 0.9 V in 4.5 M H_2SO_4 at 20°C. It can be seen from Fig. 4 that the current of Pb–Ca–Sn–Ce grid decreases more quickly than that of Pb–Ca–Sn grid in the initial period. The steady current for Pb–Ca–Sn–Ce grid, ca. 0.047 mA, is smaller than that of Pb–Ca–Sn grid, ca. 0.068 mA. It suggests that cerium improve the corrosion resistance of the alloy.

3.5. Scanning electron micrographs

After the Pb–Ca–Sn and Pb–Ca–Sn–Ce electrodes were anodized at 20°C under a constant potential of 0.90 V for 30 days, the surface of the corrosion layer was rinsed with distilled water, dried with filter paper, and examined by scanning electron microscopy. Fig. 5 shows the SEM photographs of the surface of the corrosion layers for Pb–Ca–Sn and Pb–Ca–Sn–Ce samples. It can be found that the size of the grains in the corrosion layer formed on Pb–Ca–Sn–Ce electrode is finer than that formed on Pb–Ca–Sn electrode. The finer microstructure of the Pb–Ca–Sn–Ce alloy may be due to the effect of the additive cerium in the alloy.

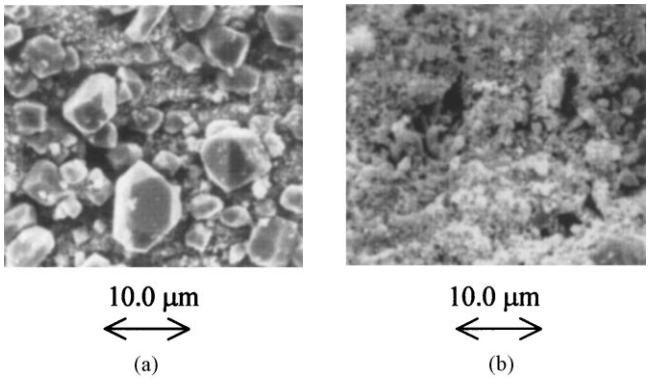

Fig. 5. Electron micrographs of the surfaces of the corrosion layers on the alloy electrodes at 0.9 V for 30 days. (a) Pb–Ca–Sn electrode, (b) Pb–Ca–Sn–Ce electrode.

4. Conclusion

The additive cerium in Pb–Ca–Sn alloy may inhibit the growth of the anodic Pb(II) and PbO_2 films, improve the corrosion resistance of the alloy and reduce the resistivity of the anodic Pb(II) film. Cerium makes the grains in the corrosion layer finer, and may, thus, inhibit the corrosion of the lead alloy.

Acknowledgements

This work was supported by the National Natural Science Foundation of China, Project no. 29873013.

References

[1] D. Pavlov, in: B.D. McNicol, D.A.J. Rand (Eds.), Power Sources for Electric Vehicles, Amsterdam, Elsevier, 1984.
[2] J.A. Bialacki, N.A. Hampson, F. Wilson, J. Appl. Electrochem. 15 (1985) 99.
[3] R.L. Cui, S.G. Wu, J. Power Sources 46 (1993) 327.
[4] B.K. Mahato, J.L. Strebe, D.F. Wilkinson, K.R. Bullock, J. Electrochem. Soc. 132 (1985) 132.
[5] D. Pavlov, J. Electrochem. Soc. 136 (1989) 27.
[6] J.L. Caillerie, L. Albert, J. Power Sources 67 (1997) 279.
[7] N. Bui, P. Mattesco, P. Simon, J. Steinmetz, E. Rocca, J. Power Sources 67 (1997) 61.
[8] H.-T. Liu, J. Yang, H.-H. Liang, W.-F. Zhou, J. Fudan Univ. (Nat. Sci.) 38 (1999) 623.
[9] N.E. Bagshaw, J. Power Sources 33 (1991) 3.
[10] H.-T. Liu, F.-W. Wang, P.-D. Xu, W.-F. Zhou, J. Fudan Univ. (Nat. Sci.) 34 (1995) 26.
[11] G.W. Mao, T.L. Wilson, J.G. Larson, J. Electrochem. Soc. 117 (1970) 1323.
[12] H.-Q. Wen, F.-C. Sheng, W.-D. Su, S.-M. Zhou, J. Power Sources 33 (1991) 21.
[13] J.R. Pierson, C.E. Weinlein, C.E. Wright, in: D.H. Collins, (Ed.), Power Sources, Vol. 5, Academic Press, London, 1975, p. 97.
[14] J. Han, C. Pu, W.-F. Zhou, J. Electroanal. Chem. 368 (1994) 43.